Cell-specific oxidative metabolism of the renal cortex

Kyle Feola[1,4], Andrea H. Venable[1,4], Tatyana Broomfield[1], Claire B. Llamas[2], Prashant Mishra[2,3], Sarah C. Huen[1]*

[1]Department of Internal Medicine (Nephrology) and Pharmacology, University of Texas Southwestern Medical Center, Dallas, Texas, USA

[2]Children's Research Institute, University of Texas Southwestern Medical Center, Dallas, Texas, USA

[3]Department of Pediatrics and the Harold C. Simmons Comprehensive Cancer Center, University of Texas Southwestern Medical Center, Dallas, Texas, USA

[4]These authors contributed equally

Running title: Renal metabolic heterogeneity

Keywords: kidney; mitochondria; metabolism; tubular epithelium; cellular metabolic heterogeneity

*Correspondence:

Sarah Huen, M.D., Ph.D.

5323 Harry Hines Blvd.

Dallas, TX 75390-9041

(214) 645-8017

sarah.huen@utsouthwestern.edu

Abstract

The metabolic health of the kidney is a primary determinant of the risk of progressive kidney disease. Our understanding of the metabolic processes that fuel kidney functions is limited by the kidney's structural and functional heterogeneity. As the kidney contains many different cell types, we hypothesize that intra-renal mitochondrial heterogeneity contributes to cell-specific metabolism. To interrogate this, we utilized a recently developed mitochondrial tagging technique to isolate kidney cell-type specific mitochondria. Here, we investigate mitochondrial functional capacities and the metabolomes of the early and late proximal tubule (PT) and the distal convoluted tubule (DCT). The conditional MITO-Tag allele was combined with *Slc34a1-CreERT2*, *Ggt1-Cre*, or *Pvalb-Cre* alleles to generate mouse models capable of cell-specific isolation of hemagglutinin (HA)-tagged mitochondria from the early PT, late PT, or the DCT, respectively. Functional assays measuring mitochondrial respiratory and fatty acid oxidation (FAO) capacities and metabolomics were performed on anti-HA immunoprecipitated mitochondria from kidneys of ad libitum fed and 24-hour fasted male mice. The renal MITO-Tag models targeting the early PT, late PT, and DCT revealed differential mitochondrial respiratory and FAO capacities which dynamically changed during fasting conditions. Changes with mitochondrial metabolomes induced by fasting suggest that the late PT significantly increases FAO during fasting. The renal MITO-Tag model captured differential mitochondrial metabolism and functional capacities across the early PT, late PT, and DCT at baseline and in response to fasting.

Translational Statement

While the renal cortex is often considered a single metabolic compartment, we discovered significant diversity of mitochondrial metabolomes and functional capacities across the proximal tubule and the distal convoluted tubule. As mitochondrial dysfunction is a major biochemical pathway related to kidney disease progression, understanding the differences in mitochondrial metabolism across distinct kidney cell populations is thus critical in the development of effective and targeted therapeutic therapies for acute and chronic kidney disease.

Introduction

Mitochondrial dysfunction has been implicated as a significant driver of disease pathology, including acute and chronic kidney disease. Recent studies have interrogated the differences of mitochondria across tissues and found significant heterogeneity in protein composition and substrate utilization, suggesting tissue-specific mitochondrial characteristics[1, 2]. As the kidney's cellular composition is diverse, it is likely that intra-renal mitochondrial heterogeneity contributes to kidney cell-specific mitochondrial function. Thus, an investigation of kidney cell-specific mitochondrial heterogeneity is needed to fully understand the mechanisms by which mitochondrial dysregulation promotes kidney disease.

The kidneys are extremely metabolically active[3], having the second highest mitochondrial density compared to other tissues[4]. While comprising 1% of total body weight, the kidneys receive 25% of cardiac output, filter 180 liters of blood daily, and consume 10% of the total body oxygen for solute transport (to maintain electrolyte, pH, and volume homeostasis) and biosynthesis (hormone production for blood pressure, red blood cell, and bone homeostasis). To perform these functions, the kidney has at least 30 distinct cell types[5]. The nephron, the basic unit of the kidney, is comprised of multiple tubular segments, the organization of which are critical to their diverse physiologic functions. Within the kidney, mitochondrial density[6] and function varies across the nephron[7]. Kidney metabolism is often simplified into a cortical and medullary 2-compartment model. Metabolic studies often use cortical slices to interrogate renal cortical metabolism. However, it is likely that cortical tubular cells, including the proximal tubule (PT) and the distal convoluted tubule (DCT), are metabolically unique as they are functionally distinct (**Figure 1A,B**). Although the PT and DCT are on different ends of the nephron, they are physical neighbors due to nephron structure. The PT is further differentiated into separate segments (S1-S3), with the early segments responsible for initial bulk transport and the S3 segment most vulnerable to ischemic and nephrotoxic insults. The metabolic profiles of these distinct cortical

tubular epithelial cells are therefore difficult to investigate in a cell-specific fashion. Current methods of interrogating kidney mitochondrial function include whole tissue mitochondrial isolation, microdissection of tubular segments, and single cell isolation using flow cytometric cell sorting with improved targeting of specific cell populations. While whole kidney mitochondrial isolation does not allow for cell-type specificity, micro dissection and flow cytometric cell sorting are limited by the need for tissue digestion and introduction of oxidative stress during the sorting process[8]. We thus sought to use the MITO-Tag system in the kidney to investigate mitochondrial properties in a kidney cell-specific manner and to determine whether mitochondrial composition and function differed among the early PT, late PT and the DCT.

Materials and Methods

Mouse Studies

All animal experiments were performed in accordance with institutional regulations after protocol review and approval by the Institutional Animal Care and Use Committee of University of Texas Southwestern Medical Center. The MITO-Tag mice[9] were bred with *Slc34a1-CreERT2*[10], *Ggt1-Cre*[11], or *Pvalb-Cre*[12] mouse lines to generate mouse models with cell type specific mitochondrial tags. MITO-Tag (RRID:IMSR_JAX:032290), *Ggt1-Cre* (RRID:IMSR_JAX:012841), and *Pvalb-Cre* (RRID:IMSR_JAX:017320) mice were purchased from Jackson Laboratory. *Slc34a1-CreERT2* (RRID:IMSR_JAX:032285) was obtained through the UT Southwestern O'Brien Research Core Center. *Slc34a1-CreERT2;MitoTag*$^{+/-}$ mice were gavaged with a single dose of tamoxifen in peanut oil (66 mg/kg body weight) and allowed a week to rest before experimental use. All mouse strains were maintained on a C57BL/6 background and housed under standard laboratory conditions with a 12:12-h light-dark cycle. Male mice were provided ad libitum access to water and standard chow (No. 2916, Harlan Teklad) or fasted for 24 hours.

Immunoprecipitation of Tagged Mitochondria

Cell specific mitochondria were isolated as described in Bayraktar EC et. al.[9]. All steps were performed at 4°C. Briefly, mouse renal tissue was homogenized in either 1 mL of KPBS (136 mM KCl, 10 mM KH_2PO_4 pH 7.25) for metabolomics and immunoblot analyses or 2 mL mitochondrial isolation buffer (5 mM HEPES, 70 mM Sucrose, 220 mM Mannitol, 5 mM $MgCl_2$, 10 mM KH_2PO_4, 1 mM EGTA, 1% fatty acid free BSA, pH 7.2) for respiration analysis. Homogenates were centrifuged for 5 minutes at 1000xg. 1 mL of supernatant was incubated with 30 µL of anti-HA beads (Thermo Scientific; 88837) for 10 minutes with rotation. HA-bead bound mitochondria were washed 2 times with 1 mL assay buffer, followed by assay specific dilution.

Isolation of Mitochondria from Whole Kidney

Mouse renal tissue was homogenized in 1 mL mitochondrial isolation buffer for respiration analysis or 1mL mitochondiral isolation buffer without BSA for immunoblot assays. Homogenates were centrifuged for 5 minutes at 600xg, followed by removal of the supernatant into a new tube. This process was repeated 6 times. Homogenates were then centrifuged for 10 minutes at 10000xg, followed by removal of the supernatant and resuspension of the pellet in 1 mL of buffer. This process was repeated two times for 5 minutes each, followed by assay specific dilution.

Antibodies

Primary antibodies used include, Calnexin (Abcam Cat# ab22595, RRID:AB_2069006); CPT1A, (Proteintech Cat# 66039-1-Ig, RRID:AB_11041710); HDAC1 (Cell Signaling Technology Cat# 5356, RRID:AB_10612242); HSP90 (Bio-Rad; VMA00082); SDHA (Cell Signaling Technology Cat# 11998, RRID:AB_2750900); SGLT2 (Abcam Cat# ab85626, RRID:AB_10674183); NCC-DL488 (StressMarq Biosciences Cat# SPC-402D-DY594, RRID:AB_2825469); PMP70 (Abcam Cat# ab85550, RRID:AB_10672335); and VDAC (Cell Signaling Technology Cat# 4661, RRID:AB_10557420). Secondary antibodies used include: donkey anti-rabbit AF488 (Thermo Fisher Scientific Cat# A-21206, RRID:AB_2535792); goat anti-chicken AF405 (Thermo Fisher Scientific Cat# A48260,

RRID:AB_2890271); donkey anti-mouse AF488 (Thermo Fisher Scientific Cat# A-21202, RRID:AB_141607), donkey anti-rabbit AF594 (Thermo Fisher Scientific Cat# A-21207, RRID:AB_141637), Anti-mouse IgG, HRP-linked Antibody (Cell Signaling Technology Cat# 7076, RRID:AB_330924), and Anti-rabbit IgG, HRP-linked Antibody (Cell Signaling Technology Cat# 7074, RRID:AB_2099233).

Immunoblotting

Mitochondria bound to anti-HA beads were incubated with triton lysis buffer (50 mM Tris HCl, 2% SDS, pH 6.8) supplemented with Halt Protease Inhibitor Cocktail (Thermo Scientific; 78443) for 20 minutes, followed by magnetization and removal of beads. Mitochondria extracted from whole tissue homogenates were resuspended in RIPA Lysis buffer (Teknova R3792) supplemented with Halt Protease Inhibitor Cocktail and incubated for 10 minutes. Protein concentration was evaluated using the DC Protein Assay kit (Bio-Rad; 5000112). Four micrograms of protein/sample were loaded into 4%–20% Mini-PROTEAN TGX stain-free polyacrylamide gels (Bio-Rad; 4568093), transferred onto PVDF membranes (Bio-Rad; 1704273), blocked in 5% milk in 1x Tris-buffered saline with 1% Tween for 1 hour, and incubated with primary antibody overnight at 4°C. Membranes were then washed and then incubated with florescent secondary antibody for 1 hour at room temperature. Either fluorescent secondary antibodies or horseradish peroxidase linked secondary antibodies with chemiluminescence (Clarity Western ECL Substrate, Bio-Rad) were used. Blots were imaged with ChemiDoc MP (Bio-Rad). Densitometry determined based on total protein quantified using Image Lab (Bio-Rad).

Immunostaining

Renal tissue was harvested and fresh frozen in OCT. 6 µm kidney sections were fixed with 4% paraformaldehyde for 30 minutes and simultaneously blocked and permeabilized in 5% normal donkey serum with 0.3% Triton-100 for 1 hour at room temperature. Tissue slides were incubated overnight with primary antibody in blocking solution overnight at 4°C, followed by incubation with secondary

antibody, DAPI (Invitrogen 62248) and/or Lotus lectin flourescein (Vector Laboratories FL 13212) in blocking solution at 1:500, 1:5000, and 1:100 dilutions, respectively, for 1 hour at room temperature. Images of immunostained sections were acquired using the LSM 880 confocal microscope (Zeiss) or a Nikon Eclipse 80i microscope using a Nikon DS-Fi3 camera. Images were processed using ImageJ2 using the Fiji image processing package.

Mitochondrial Respiration

Mitochondrial respiration was measured using the Agilent Seahorse (Seahorse XFe96 Extracellular Flux Analyzer) via the UT Southwestern Children's Medical Center Research Institute Metabolomics Core. Briefly, isolated mitochondria either bound to HA-beads or extracted from whole tissues homogenates were evaluated for protein concentration using the DC Protein Assay kit (Bio-Rad). Specific amounts of mitochondria based on assayed substrates were then resuspended in 20 µL of mitochondrial isolation buffer and plated onto a 96-well plate: 1 µg/well for Complex II function (5 mM succinate/2 µM rotenone); 2 µg/well for CPT1-independent FAO (50 µM palmitoylcarnitine/0.5 mM malate); 2.5 µg/well for CPT1-dependent FAO (40 µM Palmitoyl-CoA/0.5 mM Carnitine/0.5 mM Malate). After plating mitochondria, the 96-well plate with added mitochondria was centrifuged for 2 minutes at 2,700xg at 4°C. Buffer with or without substrate mixture (130 µL) was added to each well. Oxygen consumption rate (OCR) was measured as follows: baseline measurements were taken for 6 minutes; followed by treatment with 4 mM adenosine diphosphate (ADP) and measurement for 3 minutes; followed by treatment with 2 µM Oligomycin and measurement for 5 minutes; followed by treatment with 2 µM carbonyl cyanide m-chlorophenyl hydrazone (CCCP) and measurement for 3 minutes; followed by treatment with either 2 µM Antimycin A or 10 µM Cytochrome C. Subsequent analysis was performed using the Agilent Wave XF Software v2.6.1.

Metabolomics

HA-bead bound mitochondria were incubated in LC/MS extraction buffer (80% methanol/20% LC/MS water) and samples frozen at -80°C until targeted screening metabolomic analysis was performed by the UT Southwestern Children's Medical Center Research Institute Metabolomics Core. Data acquisition was performed by reverse-phase chromatography on a 1290 UHPLC liquid chromatography (LC) system interfaced to a high-resolution mass spectrometry (HRMS) 6550 iFunnel Q-TOF mass spectrometer (MS) (Agilent Technologies, CA). The MS was operated in both positive and negative (ESI+ and ESI-) modes. Analytes were separated on an Acquity UPLC® HSS T3 column (1.8 µm, 2.1 x 150 mm, Waters, MA). The column was kept at room temperature. Mobile phase A composition was 0.1% formic acid in water and mobile phase B composition was 0.1% formic acid in 100% ACN. The LC gradient was 0 min: 1% B; 5 min: 5% B; 15 min: 99%; 23 min: 99%; 24 min: 1%; 25 min: 1%. The flow rate was 250 µL min-1. The sample injection volume was 5 µL.

ESI source conditions were set as follows: dry gas temperature 225 °C and flow 18 L min-1, fragmentor voltage 175 V, sheath gas temperature 350 °C and flow 12 L min-1, nozzle voltage 500 V, and capillary voltage +3500 V in positive mode and −3500 V in negative. The instrument was set to acquire over the full m/z range of 40–1700 in both modes, with the MS acquisition rate of 1 spectrum s-1 in profile format.

Raw data files (.d) were processed using Profinder B.08.00 SP3 software (Agilent Technologies, CA) with an in-house database containing retention time and accurate mass information on 600 standards from Mass Spectrometry Metabolite Library (IROA Technologies, MA) which was created under the same analysis conditions. The in-house database matching parameters were: mass tolerance 10 ppm; retention time tolerance 0.5 min. Peak integration result was manually curated in Profinder for improved consistency and exported as a spreadsheet (.csv). Data normalized by the total ion count (Supplemental Table 1).

Heat map, Partial Least Squares-Discriminant Analysis (PLS-DA), and Variable Importance in Projection (VIP) score, and Kyoto Encyclopedia of Genes and Genomes (KEGG) analyses and plots were generated using Metaboanalyst.ca.

Statistical Analysis

Statistical analyses were performed using Prism 10.0 (GraphPad). One-way ANOVA with Bennett's multiple comparison analysis and Two-way ANOVA with Sidak's multiple comparison analysis was used to compare mitochondrial OCR and western blot protein densitometry across groups and conditions. Statistical analysis for metabolomics described above. A P value < 0.05 was considered statistically significant. Prism 10.0 (GraphPad), Illustrator (Adobe), and BioRender.com were used to generate figures.

Results and Discussion

Isolation of kidney cell-specific mitochondria from cortical tubular cells

The MITO-Tag mouse model[9] was developed to isolate mitochondria from tissues in a cell-specific manner. Cre recombinase activity leads to expression of an HA-tagged construct of an outer mitochondrial protein (3xHA-eGFP-OMP25) allowing for immuno-isolation of mitochondria using anti-HA beads (**Figure 1C**). In comparison to whole tissue mitochondrial isolation which requires multiple centrifugation steps and could require up to an hour, MITO-Tag mitochondria isolation could be accomplished within minutes. In order to isolate mitochondria from the early PT, we generated the *Slc34a1-CreERT2;MITO-Tag* (Slc34a1-MT) mouse model. The *Slc34a1-CreERT* inducible model[10] with tamoxifen dose dependent efficiency allows for targeting the early S1-S2 segment of the kidney with one dose of tamoxifen. Co-localization of MITO-Tag expression with predominantly sodium glucose co-transporter 2 (SGLT2)-expressing proximal tubule cells is seen in Slc34a1-MT kidneys (**Figure 1D**). The *Ggt1-Cre;MITO-Tag* (Ggt-MT) mouse model[11] was used to isolate mitochondria from the late PT, the S2-S3 segment (**Figure 1D**). MITO-Tag does not co-localize with SGLT2-expressing cells in Ggt-

MT kidneys. We next generated the *PvAlb-Cre;MITO-Tag* (PvAlb-MT) mouse model which allows for the isolation of early DCT (DCT1) mitochondria[13] (**Figure 1D**). In PvAlb-MT kidneys, MITO-Tag expression co-localizes with the DCT-specific transporter, NCC. All three models show enrichment of mitochondria, but not nuclear or cytoplasmic components, using anti-HA immunoprecipitation (**Figure 2A**).

Contact sites are well known between mitochondria other organelles, particularly the endoplasmic reticulum (ER) and peroxisomes[14]. Similar to a hepatic MITO-Tag model[9] and traditional whole tissue mitochondrial isolation, anti-HA MITO-Tag immunoprecipitation with our renal MITO-Tag models also enriched for both ER and peroxisomes (**Figure 2B**). Immunostaining shows co-localization of MITO-Tag expression with calnexin (ER) and PMP70 (peroxisome) in Slc34a1-MT, Ggt-MT, and PvAlb-MT kidneys (**Figure 2C**).

Differential mitochondrial functional and fatty acid oxidative capacities

In order to test mitochondrial viability, we compared the respiratory response to cytochrome c between MITO-Tag isolated mitochondria and whole kidney mitochondria isolated using traditional methods. Similar to whole kidney isolated mitochondria, the MITO-Tag isolated mitochondria exhibited a minimal increase in respiration in the presence of cytochrome c[15], suggesting that the mitochondrial outer membrane using the rapid MITO-Tag isolation protocol remained largely intact (**Figure 3A**).

As mitochondrial function has been described to be unique across organs[1], we next examined whether the functional capacities of mitochondria vary across different tubular segments. To assess mitochondrial function, we isolated Slc34a1-MT, Ggt-MT, and PvAlb-MT mitochondria and measured their respiratory capacity. For each substrate, oxygen consumption was measured without ADP (State IV respiration) and with ADP (State III respiration). Measuring Complex II activity with succinate as the substrate (with rotenone to inhibit Complex I activity), we observed robust induction of mitochondrial

respiration with the addition of ADP (**Figure 3B**). Across the three renal tubular cortical segments, there is a slight difference in Complex II activity, with the early PT having the lowest State III respiration. As it has been described that liver mitochondria decrease Complex II activity after an overnight fast[16], we next measured the respiratory capacities after 24 hours of fasting. Interestingly, fasting does not change Complex II activity in late PT mitochondria, however fasting significantly decreases Complex II activity in DCT mitochondria (**Figure 3C,D**). As fatty acid oxidation (FAO) is a key metabolic pathway in kidney health[17], we next examined segment-specific FAO capacity. Using palmitoylcarnitine as the substrate (**Figure 3E**), we found that the late PT has the highest FAO capacity compared to the early PT and DCT (**Figure 3F**).

Dynamic and renal cell-specific metabolome

As the mitochondrial functional capacities differed across these three renal segments, we next performed metabolomic analysis on segment-specific MITO-Tag isolated mitochondria and associated mitochondrial membranes. Metabolite signatures were unique in fed and fasted conditions across the early PT, late PT, and DCT based on Partial Least-Squares Discriminant Analysis (PLS-DA) (**Figure 4A**). Pathway analysis of the metabolomic data revealed differences in metabolic processes across these three segments, including differences in lipid and amino acid metabolism (**Figure 4B**). In response to fasting, significant metabolic changes were observed within each segment (**Figure 4C**). Interestingly, abundances of acylcarnitines and acetylcarnitine increase significantly after fasting primarily within the late PT, while no changes are observed in the DCT (**Figure 4D,E**).

The PT is classically described to preferentially use fatty acids for energy as compared to the DCT, although the DCT does express genes involved in FAO[6, 18, 19]. While acylcarnitines are a key starting substrate for FAO, long chain fatty acids must be transported into the mitochondria as an acylcarnitine via carnitine palmitoyltransferase 1 (CPT1), the rate limiting enzyme of FAO[20]. Interestingly, single-cell RNA sequencing data suggest that *Cpt1a*, which encodes CPT1A is more highly expressed in the DCT

than in the PT[5]. At the protein level, CPT1A is not significantly different across the early PT, late PT, and DCT (**Figure 5A,B**). In the prior studies assessing FAO capacity we had used palmitoylcarnitine (**Figure 3F**), which bypasses the need for CPT1 transport into mitochondria[21]. To determine whether CPT1 contributed to the differential changes in acylcarnitine abundance we observed during fasting, we measured mitochondrial oxygen consumption using palmitoyl-CoA, a long chain acyl-CoA that requires CPT1 for transport into the mitochondria (**Figure 3E**). We focused on the late PT and DCT as we observed a significant increase in acylcarnitines during fasting in the late PT, while there were no changes in the DCT. Despite similar CPT1A protein abundances, the DCT has much lower CPT1-dependent FAO capacity compared to the late PT (**Figure 5C**). Consistent with an increase in FAO during fasting[22], palmitoyl-CoA oxidation significantly increases in the late PT, while there is a small non-significant increase in the DCT. While increases in acylcarnitines are often attributed to defects in FAO[23], it is well-established that acylcarnitines can also increase as a physiologic response to fasting[24, 25]. In context with the above FAO capacity measurements, acylcarnitine production is likely enhanced in the late PT in response to fasting, increasing substrates to maximize downstream FAO.

To highlight the power of this kidney cell-specific mitochondrial system, we compared the difference in FAO measurements between mitochondria isolated from a whole kidney homogenate using traditional methods and immunoprecipitated late PT- and DCT-specific mitochondria. Similar to DCT-specific mitochondria, a mixture of mitochondria isolated from the whole kidney exhibit a modest non-significant increase in palmitoyl-CoA oxidation in the fasted state compared to the fed state (**Figure 5C**). These data suggest that differences in FAO at a kidney cell-specific level and the magnitude of the changes that occur in response to a metabolic stress cannot be captured by a mixed population of isolated mitochondria at the whole kidney level.

Limitations and Future Directions

While the kidney MITO-Tag system can elucidate the mitochondrial heterogeneity across the diverse landscape of the many kidney cell types, there are some limitations to our model. First, as peroxisomes are co-isolated with the MITO-Tag system, the metabolomics and FAO measurements cannot fully differentiate between mitochondrial and peroxisomal metabolism. Moreover, peroxisomes are more abundant in the PT (**Figure 2C**) and could compensate in the context of tubular CPT1A deficiency[26]. While it has been described that peroxisomes can accept palmitoylcarnitine as a substrate in the context of mitochondrial FAO defects, peroxisomal oxidation of palmitoylcarnitine is estimated at only ~2% of whole cell activity[27]. Moreover, the level of non-mitochondrial oxygen consumption in response to palmitoyl-CoA is similar, if not lower, in the MITO-Tag isolated mitochondria compared to that of mitochondria isolated from the whole kidney using traditional methods (**Figure 5D**). Interestingly, the contribution of non-mitochondrial oxygen consumption in MITO-Tag isolated mitochondria from fasted mice is even lower, suggesting that the increase in FAO capacity observed in late PT and DCT mitochondria in response to fasting is driven primarily from mitochondria. Thus, our findings suggesting differential acyl-CoA FAO metabolism in the context of fasting is likely driven primarily by mitochondrial metabolism, with a potential minor contribution from peroxisomes. Second, we leveraged the tamoxifen dose dependence to enrich for early S1-S2 PT cells, however, the *Slc34a1-CreERT2* and *Ggt1-Cre* are not exact in their targeting of the S1, S2, and S3 segments of the proximal tubule. *PvAlb-Cre* driver only targets the early DCT. Future work is needed to investigate the metabolic differences between DCT1 and DCT2, as well as other renal cell types. Third, the studies presented here were performed in male mice. Future work will investigate kidney cell-specific sexual dimorphism of mitochondrial metabolism which has been reported in other tissues[28, 29]. Fourth, our studies focused primarily on lipid metabolism and FAO. Future work is needed to address kidney cell-specific amino acid metabolism as highlighted as differentially abundant (**Figure 4B**). Finally, inherent to the MITO-Tag method is the removal of the mitochondria from the in vivo environment. Future research is needed to incorporate technologies such as MALDI-MSI[30] to integrate spatial metabolomics with the ex vivo renal MITO-Tag functional studies.

Conclusion

The renal MITO-Tag model has the power of interrogating kidney cell-specific mitochondrial function. This ability to measure kidney cell-specific metabolism can be transformative and enable the advancement in several key areas of kidney research, including kidney development, physiology, disease pathogenesis and mitochondrial biology and therapeutics. Using this system, we have for the first time defined the mitochondrial metabolic heterogeneity of renal cortical tubular epithelium and discovered differential FAO capacities of the early PT, late PT and the DCT.

Disclosure Statement

No conflicts of interest, financial, or otherwise, are declared by the authors.

Data Statement

Metabolomic data is available in Supplemental Table 1. All other data related to the manuscript will be made available upon request.

Acknowledgements

This work was supported by funding from the National Institute of General Medical Sciences (R35GM137984 to S.C.H.), National Institute of Diabetes and Digestive and Kidney Diseases (R56DK134582, R01DK135555 to S.C.H. and T32DK007257 to A.H.V), the National Institutes of Health (DP2ES030449 and R01AR073217 to P.M.), the Moody Medical Research Institute (Research Grant to P.M.), and the King Foundation (Research Grant to P.M.).

Author Contributions

Conceptualization/Design: K.F., A.H.V., S.C.H., Investigation: K.F., A.H.V., C.L., (with assistance from T.B.), Analysis: K.F., A.V., P.M., S.C.H., Writing–Original Draft: S.C.H., Writing–Review/Editing: K.F., A.V., P.M., S.C.H. All authors approved the final manuscript.

References

1. McLaughlin KL, Hagen JT, Coalson HS et al. Novel approach to quantify mitochondrial content and intrinsic bioenergetic efficiency across organs. *Sci Rep*. 2020; 10: 17599.
2. Kappler L, Hoene M, Hu C et al. Linking bioenergetic function of mitochondria to tissue-specific molecular fingerprints. *Am J Physiol Endocrinol Metab*. 2019; 317: E374-E387.
3. Bhargava P, Schnellmann RG. Mitochondrial energetics in the kidney. *Nat Rev Nephrol*. 2017; 13: 629-646.
4. Pagliarini DJ, Calvo SE, Chang B et al. A mitochondrial protein compendium elucidates complex I disease biology. *Cell*. 2008; 134: 112-123.
5. Ransick A, Lindström NO, Liu J et al. Single-Cell Profiling Reveals Sex, Lineage, and Regional Diversity in the Mouse Kidney. *Dev Cell*. 2019; 51: 399-413.e7.
6. Kone BC. Metabolic Basis of Solute Transport. In: Brenner BM, ed. *Brenner & Rector's The Kidney*. 2008:130-155.
7. Hall AM, Unwin RJ, Parker N, Duchen MR. Multiphoton imaging reveals differences in mitochondrial function between nephron segments. *J Am Soc Nephrol*. 2009; 20: 1293-1302.
8. Llufrio EM, Wang L, Naser FJ, Patti GJ. Sorting cells alters their redox state and cellular metabolome. *Redox Biol*. 2018; 16: 381-387.
9. Bayraktar EC, Baudrier L, Özerdem C et al. MITO-Tag Mice enable rapid isolation and multimodal profiling of mitochondria from specific cell types in vivo. *Proc Natl Acad Sci U S A*. 2019; 116: 303-312.
10. Kusaba T, Lalli M, Kramann R, Kobayashi A, Humphreys BD. Differentiated kidney epithelial cells repair injured proximal tubule. *Proc Natl Acad Sci U S A*. 2014; 111: 1527-1532.

11. Iwano M, Plieth D, Danoff TM, Xue C, Okada H, Neilson EG. Evidence that fibroblasts derive from epithelium during tissue fibrosis. *J Clin Invest*. 2002; 110: 341-350.

12. Hippenmeyer S, Vrieseling E, Sigrist M et al. A developmental switch in the response of DRG neurons to ETS transcription factor signaling. *PLoS Biol*. 2005; 3: e159.

13. Chen L, Chou CL, Knepper MA. Targeted Single-Cell RNA-seq Identifies Minority Cell Types of Kidney Distal Nephron. *J Am Soc Nephrol*. 2021; 32: 886-896.

14. Murley A, Nunnari J. The Emerging Network of Mitochondria-Organelle Contacts. *Mol Cell*. 2016; 61: 648-653.

15. Lee AC, Zizi M, Colombini M. Beta-NADH decreases the permeability of the mitochondrial outer membrane to ADP by a factor of 6. *J Biol Chem*. 1994; 269: 30974-30980.

16. Menezes-Filho SL, Amigo I, Luévano-Martínez LA, Kowaltowski AJ. Fasting promotes functional changes in liver mitochondria. *Biochim Biophys Acta Bioenerg*. 2019; 1860: 129-135.

17. Kang HM, Ahn SH, Choi P et al. Defective fatty acid oxidation in renal tubular epithelial cells has a key role in kidney fibrosis development. *Nat Med*. 2015; 21: 37-46.

18. Wirthensohn G, Guder WG. Renal substrate metabolism. *Physiol Rev*. 1986; 66: 469-497.

19. Guder WG, Ross BD. Enzyme distribution along the nephron. *Kidney Int*. 1984; 26: 101-111.

20. McGarry JD, Foster DW. Regulation of hepatic fatty acid oxidation and ketone body production. *Annu Rev Biochem*. 1980; 49: 395-420.

21. Ojuka E, Andrew B, Bezuidenhout N et al. Measurement of β-oxidation capacity of biological samples by respirometry: a review of principles and substrates. *Am J Physiol Endocrinol Metab*. 2016; 310: E715-23.

22. Schulz H. *"Fatty Acid Oxidation", Encyclopedia of Biological Chemistry (Second Edition)*. Academic Press; 2013.

23. Kler RS, Jackson S, Bartlett K et al. Quantitation of acyl-CoA and acylcarnitine esters accumulated during abnormal mitochondrial fatty acid oxidation. *J Biol Chem*. 1991; 266: 22932-22938.

24. Frohlich J, Seccombe DW, Hahn P, Dodek P, Hynie I. Effect of fasting on free and esterified carnitine levels in human serum and urine: correlation with serum levels of free fatty acids and beta-hydroxybutyrate. *Metabolism*. 1978; 27: 555-561.

25. Hoppel CL, Genuth SM. Carnitine metabolism in normal-weight and obese human subjects during fasting. *Am J Physiol*. 1980; 238: E409-15.

26. Hammoud S, Ivanova A, Osaki Y et al. Tubular CPT1A deletion minimally affects aging and chronic kidney injury. *JCI Insight*. 2024; 9: e171961.

27. Violante S, Achetib N, van Roermund CWT et al. Peroxisomes can oxidize medium- and long-chain fatty acids through a pathway involving ABCD3 and HSD17B4. *FASEB J*. 2019; 33: 4355-4364.

28. Norheim F, Hasin-Brumshtein Y, Vergnes L et al. Gene-by-Sex Interactions in Mitochondrial Functions and Cardio-Metabolic Traits. *Cell Metab*. 2019; 29: 932-949.e4.

29. MacCannell ADV, Futers TS, Whitehead A, Moran A, Witte KK, Roberts LD. Sexual dimorphism in adipose tissue mitochondrial function and metabolic flexibility in obesity. *Int J Obes (Lond)*. 2021; 45: 1773-1781.

30. Wang G, Heijs B, Kostidis S et al. Analyzing cell-type-specific dynamics of metabolism in kidney repair. *Nat Metab*. 2022; 4: 1109-1118.

Figure 1

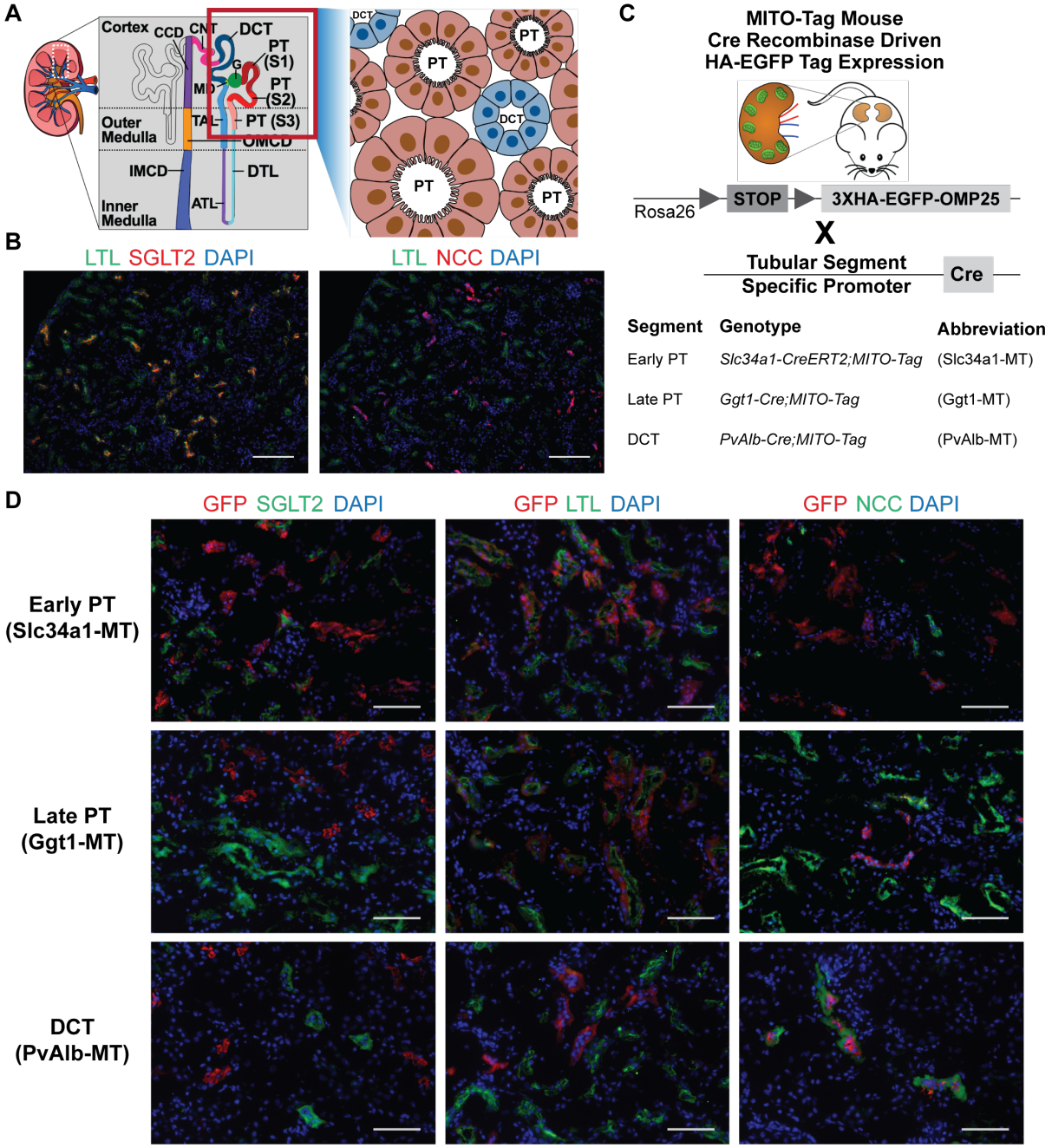

Figure 1. A model to study renal tubular mitochondrial heterogeneity.
A. Schematic of the heterogeneous renal tubular epithelium. Inset highlights the juxtaposition of proximal tubular (PT) and distal convoluted tubular (DCT) cells.
B. Immunostaining with sodium glucose co-transporter 2 (SGLT2, early PT S1-S2 segment), Lotus lectin (LTL, PT S1-S2>S3) and sodium chloride co-transporter (NCC, DCT). Scale bar = 100 µm.
C. MITO-Tag mouse models to target the Early PT, Late PT, and DCT.

D. Immunostaining with anti-GFP (anti-HA MITO-Tag includes GFP construct), SGLT2, LTL, and NCC of Slc34a1-MT, Ggt1-MT, and PvAlb-MT kidneys. Scale bar = 50 μm.

Figure 2

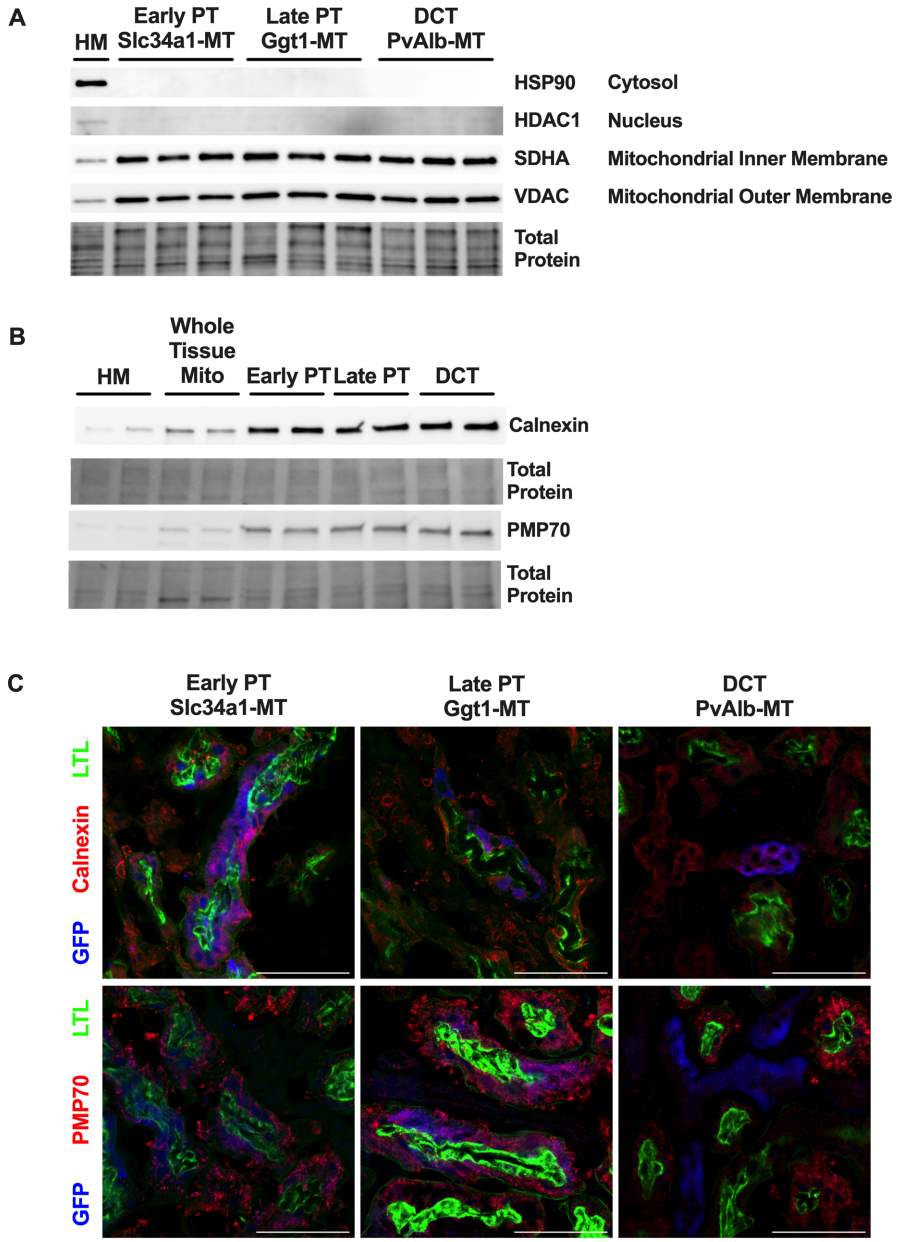

Figure 2. Isolation of intact kidney cell specific mitochondria
A. Immunoblot of protein samples of whole kidney homogenate (HM) and mitochondria isolated via anti-HA immunoprecipitation from Slc34a1-MT, Ggt1-MT, and PvAlb-MT kidneys.
B. Immunoblot of protein samples of whole kidney homogenate (HM), mitochondria isolated from whole kidney (whole tissue mito), and mitochondria isolated via anti-HA immunoprecipitation from Slc34a1-MT, Ggt1-MT, and PvAlb-MT kidneys.
C. Immunostaining with anti-GFP (MITO-Tag), Calnexin (endoplasmic reticulum), PMP70 (peroxisome), and LTL of Slc34a1-MT, Ggt1-MT, and PvAlb-MT kidneys. Scale bar = 50 μm.

Figure 3

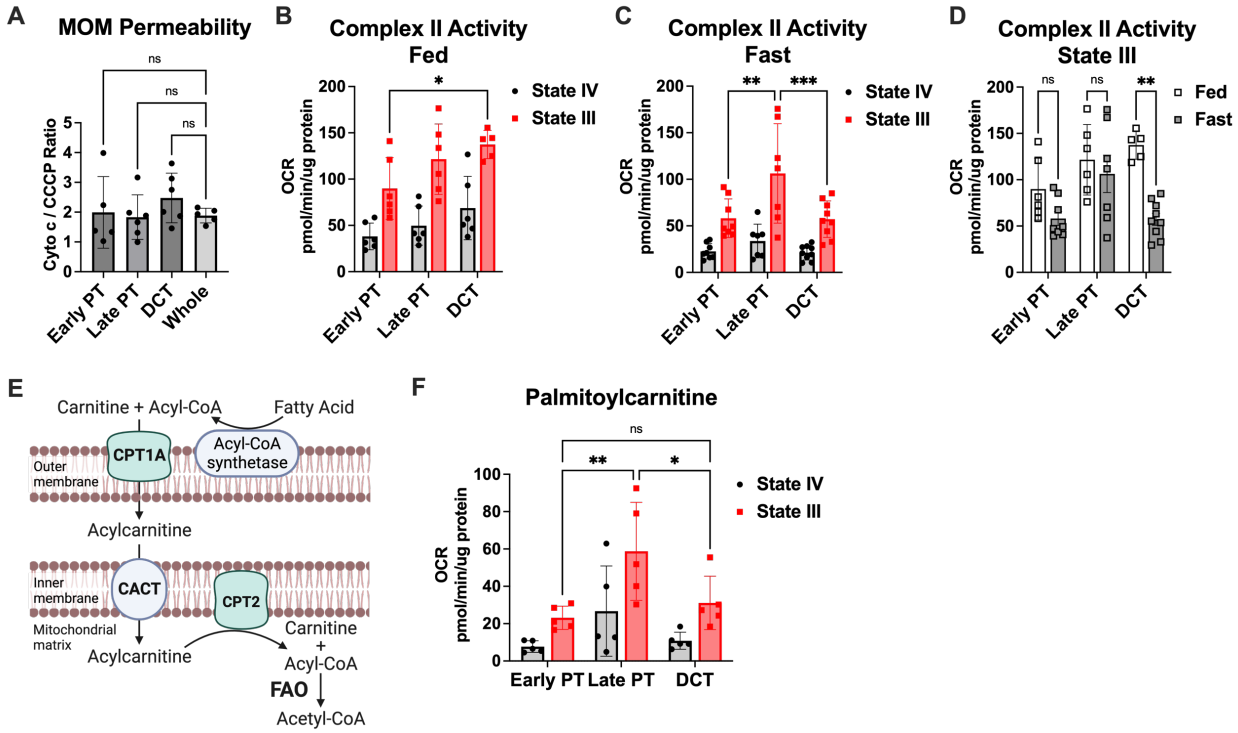

Figure 3. Differential and fasting-induced changes in mitochondrial respiratory and fatty acid oxidation capacities in the proximal tubule and the distal convoluted tubule.
A-D,F. Mitochondria were isolated via anti-HA immunoprecipitation from Slc34a1-MT (Early PT), Ggt1-MT (Late PT), and PvAlb-MT (DCT) kidneys from fed or 24-hour fasted mice. Data shown as mean±SD.
A-D. Mitochondrial respiration measured by oxygen consumption rate (OCR) using Complex II substrate (5 mM Succinate) with a Complex I inhibitor (2 μM Rotenone) before (State IV) and after 4 mM ADP (State III), n=5-7/group.
A. Mitochondria isolated from fed mice. Mitochondrial outer membrane (MOM) permeability measured by oxygen consumption rate (OCR) using Complex II substrate (5 mM Succinate) with cytochrome c treatment after treatment with an uncoupler (CCCP). Data shown as ratio of cytochrome c OCR versus CCCP OCR. MITO-Tag mitochondria compared to isolated mitochondria from whole kidney (Whole).
B-D. Comparison of State III respiration across early PT, late PT, and DCT segments and between fed and fasted states.
E. Diagram of carnitine palmitoyltransferase 1 (CPT1) converting long-chain acyl-CoA species to their respective long-chain acylcarnitines for transport into the mitochondria.
F. Fatty acid oxidation (FAO) capacity measured by OCR using 50 μM palmitoylcarnitine as a substrate, before (State IV) and after 4 mM ADP (State III), n=5/group.
A. One-way ANOVA with Bennett's multiple comparisons test, ns, not significant.
B-D,F. Two-way ANOVA with Tukey's multiple comparisons test, *P<0.05, **P<0.01, ***P<0.001.

Figure 4

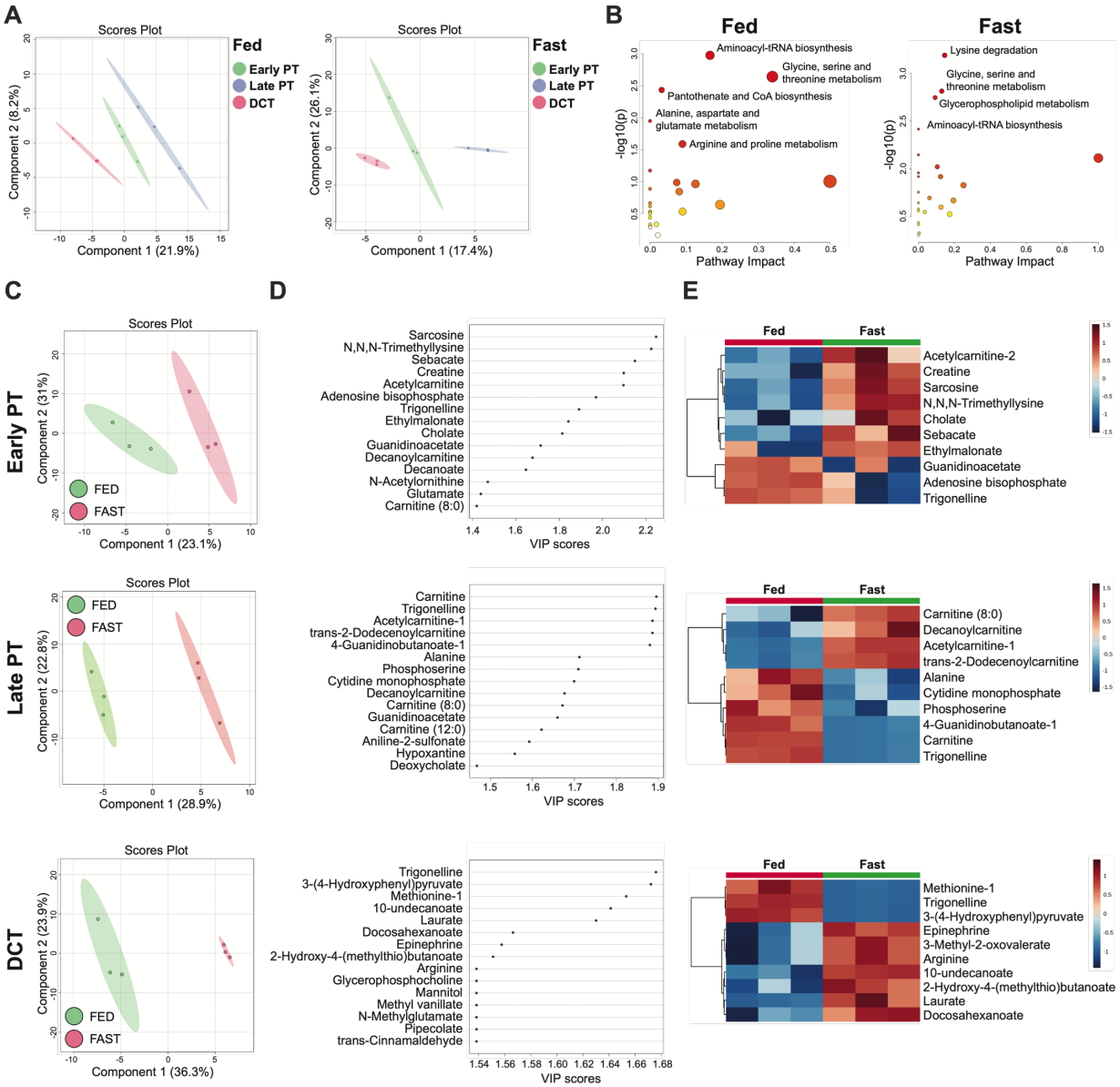

Figure 4. Differential and fasting-induced changes in mitochondrial metabolite composition in the proximal tubule and the distal convoluted tubule.
Mitochondria isolated via anti-HA immunoprecipitation from Slc34a1-MT (Early PT), Ggt1-MT (Late PT), and PvAlb-MT (DCT) kidneys from fed or 24-hour fasted mice were submitted for targeted screening metabolomics by LC/MS-MS, n=3/group. Analysis performed via Metaboanalyst, details described in Methods.
A. Partial Least Squares-Discriminant Analysis (PLS-DA) of metabolites across the early PT, late PT, and DCT in fed and fasted conditions.

B. KEGG pathway analysis of metabolites across the early PT, late PT, and DCT in fed and fasted conditions.
C. PLS-DA of metabolites in fed versus fasted conditions within each segment.
D. Variable importance in projection (VIP) scores for metabolites in fed versus fasted conditions within each segment.
E. Heatmap of relative normalized abundances of mitochondrial metabolites in fed versus fasted conditions within each segment.

Figure 5.

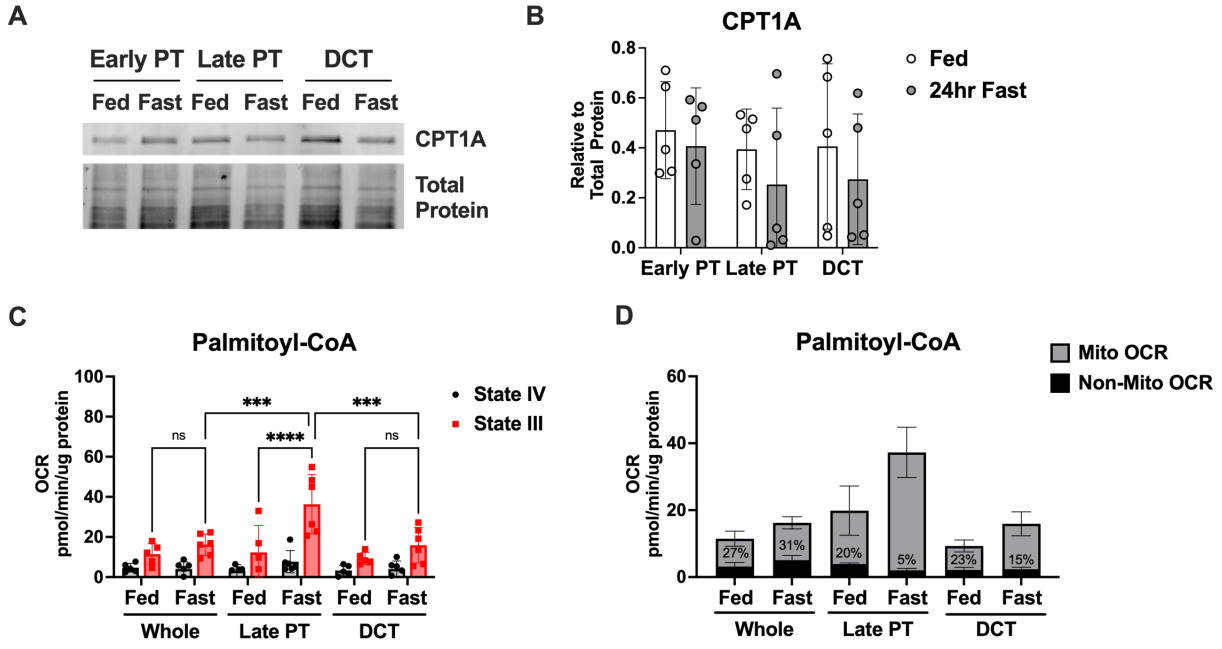

Figure 5. Differential CPT1-dependent fatty acid oxidation relative to CPT1A protein abundance.

A. Representative immunoblot of protein samples of mitochondria isolated via anti-HA immunoprecipitation.

B. Densitometry of (A), n=5/group, no comparison was significantly different.

C-D. Mitochondria were isolated via traditional whole kidney tissue isolation (whole) or anti-HA immunoprecipitation from Ggt1-MT (Late PT) and PvAlb-MT (DCT) kidneys from fed or 24-hour fasted mice.

C. FAO capacity measured by OCR using 40 μM palmitoyl-CoA as a substrate, before (State IV) and after 4 mM ADP (State III), n=5-6/group.

D. After ADP-stimulation, OCR measured after treatment with antimycin A, which specifically inhibits mitochondrial function, is the non-mitochondrial contribution to OCR. Percentages shown on bar graph represent the percent contribution of non-mitochondrial OCR.

B,C. Data shown as mean±SD. Two-way ANOVA with Tukey's multiple comparisons test, ***P<0.001, ****P<0.0001.

Supplemental Table 1. Targeted metabolomics of renal cortical cell-specific mitochondria in fed and fasted states.

Mitochondria isolated via anti-HA immunoprecipitation from Slc34a1-MT (Slcfed, Slcfast), Ggt1-MT (Ggtfed, Ggtfast), and PvAlb-MT (PvAfed, PvAfast) kidneys from fed or 24-hour fasted mice were submitted for targeted screening metabolomics by LC/MS-MS, n=3/group. Data shown as normalized to total ion count.